New Phytologist

Research

Tandem gene amplification restores photosystem II accumulation in cytochrome b_{559} mutants of cyanobacteria

Yi-Fang Chiu[1], Han-Yi Fu[1], Petra Skotnicová[2], Keng-Min Lin[1], Josef Komenda[2] and Hsiu-An Chu[1]

[1]Institute of Plant and Microbial Biology, Academia Sinica, Taipei 11529, Taiwan; [2]Laboratory of Photosynthesis, Centre Algatech, Institute of Microbiology of the Czech Academy of Sciences, Třeboň 379 01, Czech Republic

Authors for correspondence:
Josef Komenda
Email: komenda@alga.cz

Hsiu-An Chu
Email: chuha@gate.sinica.edu.tw

Received: *23 June 2021*
Accepted: *30 September 2021*

New Phytologist (2021)
doi: 10.1111/nph.17785

Key words: cyanobacterium, cytochrome b_{559}, photosynthesis, photosystem II (PSII), tandem gene amplification.

Summary

- Cytochrome (Cyt) b_{559} is a key component of the photosystem II complex (PSII) that is essential for its proper functioning and assembly. Site-directed mutants of the model cyanobacterium *Synechocystis* sp. PCC6803 with mutated heme axial ligands of Cyt b_{559} have little PSII and are therefore unable to grow photoautotrophically.
- Here we describe two types of *Synechocystis* autotrophic transformants that retained the same mutations in Cyt b_{559} but are able to accumulate PSII and grow photoautotrophically. Whole-genome sequencing revealed that all of these autotrophic transformants carried a variable number of tandem repeats (from 5 to 15) of chromosomal segments containing the *psbEFLJ* operon.
- RNA-seq analysis showed greatly increased transcript levels of the *psbEFLJ* operon in these autotrophic transformants. Multiple copies of the *psbEFLJ* operon in these transformants were only maintained during autotrophic growth, while its copy numbers gradually decreased under photoheterotrophic conditions. Two-dimensional PAGE analysis of membrane proteins revealed a strong deficiency in PSII complexes in the Cyt b_{559} mutants that was reversed in the autotrophic transformants.
- These results illustrate how tandem gene amplification restores PSII accumulation and photoautotrophic growth in Cyt b_{559} mutants of cyanobacteria, and may serve as an important adaptive mechanism for cyanobacterial survival.

Introduction

Photosystem II (PSII) is a large multisubunit pigment–protein complex located in the thylakoid membranes of cyanobacteria, algae, and plants (Barber, 2006; Umena *et al.*, 2011). This complex utilises light energy to extract electrons from water and drive the transfer of electrons to plastoquinone, which is accompanied by the release of oxygen as a byproduct.

The PSII reaction centre complex (RCII) consists of the protein subunits D1, D2, cytochrome b_{559} (Cyt b_{559}), and PsbI (Barber, 2006; Umena *et al.*, 2011). The chlorophyll (Chl)*a*-binding proteins CP47 and CP43 associate with RCII and function as the core antenna. In addition, several (at least 14) other protein subunits (mostly low molecular weight) are associated with fully assembled PSII. The biogenesis of PSII in cyanobacteria has been described as the stepwise assembly of four preassembled pigment–protein modules (D2mod, D1mod, CP47mod, and CP43mod) into intermediate complexes, which ultimately form the functional PSII holoenzyme (Komenda *et al.*, 2004; Nixon *et al.*, 2010; Nickelsen & Rengstl, 2013; Kiss *et al.*, 2019; Zabret *et al.*, 2021). The assembly of PSII is facilitated by a number of accessory or auxiliary protein factors that are not present in the fully assembled functional PSII (Komenda *et al.*, 2004; Nixon *et al.*, 2010; Nickelsen & Rengstl, 2013; Kiss *et al.*, 2019; Zabret *et al.*, 2021).

Cyt b_{559} is a heme-bridged heterodimer protein comprising one α-subunit and one β-subunit (subunits PsbE and PsbF encoded by *psbE* and *psb F*genes, respectively) (Shinopoulos & Brudvig, 2012; Chu & Chiu, 2016; and references therein). In the model cyanobacterium *Synechocystis* sp. PCC 6803 (from this point forwards *Synechocystis*), PsbE and PsbF provide His-22 residues as axial ligands for the noncovalently bound heme of Cyt b_{559}. PSII is susceptible to photodamage, and several studies have suggested that Cyt b_{559} may participate in secondary electron transfer pathways that protect PSII against photoinhibition (Barber & De Las Rivas, 1993; Bondarava *et al.*, 2003; Shinopoulos & Brudvig, 2012; Chu & Chiu, 2016; and references therein). Cyt b_{559} subunits also interact with D2 to form the essential intermediate complex during the early steps of PSII assembly (Komenda *et al.*, 2004; Kiss *et al.*, 2019). This concept has been supported by mutagenesis studies in *Synechocystis*, the green alga *Chlamydomonas reinhardtii*, and tobacco (*Nicotiana tabacum*), all showing that the assembly of active PSII reaction centres requires the presence of both the α- and β-subunits of Cyt b_{559} (Pakrasi *et al.*, 1988; Morais *et al.*, 1998; Swiatek *et al.*, 2003).

© 2021 The Authors
New Phytologist © 2021 New Phytologist Foundation
This is an open access article under the terms of the Creative Commons Attribution-NonCommercial-NoDerivs License, which permits use and distribution in any medium, provided the original work is properly cited, the use is non-commercial and no modifications or adaptations are made.

To investigate the exact physiological function of Cyt b_{559} in PSII in *Synechocystis*, several mutagenesis studies were performed to characterise a series of site-directed mutants with mutations in the His-22 residues of PsbE and PsbF (Pakrasi *et al.*, 1991; Hung *et al.*, 2007). Most of these Cyt b_{559} mutants did not accumulate a sufficient amount of active PSII and therefore were unable to grow photoautotrophically. These findings suggest that the coordination of the heme cofactor in Cyt b_{559} is important for the assembly or stability of PSII in *Synechocystis* (Pakrasi *et al.*, 1991; Hung *et al.*, 2007, 2010). Interestingly, we previously identified several spontaneously generated autotrophic transformants/pseudorevertants during the segregation of a Cyt b_{559} mutant on agar plates (Hung *et al.*, 2007). However, how these strains restored their ability for photoautotrophic growth was unclear.

In the present study, we report the characterisation of several previously identified Cyt b_{559} autotrophic transformants as well as newly generated autotrophic transformants using an antenna attenuation method (Fig. 1). We performed whole-genome sequencing, genomic DNA analysis, RNA sequencing (RNA-seq), and two-dimensional protein analysis on both groups of Cyt b_{559} transformants to reveal how they regained their ability to accumulate PSII and grow photoautotrophically. This study reveals a novel survival mechanism used by cyanobacteria to overcome mutation-induced instability of important protein components.

Materials and Methods

Mutant strains and growth conditions

Wild-type (WT) and most Cyt b_{559} mutant stains used in this study were generated and described previously (Hung *et al.*, 2007). The original H22Kα mutant strain (H22KαPS+) (Hung *et al.*, 2007) carried the tandem amplification of chromosomal segments containing the *psbEFLJ* operon. We generated the new H22Kα mutant strain by transforming the mutant plasmid into the host strain (ΔpsbEFLJ) as described (Hung *et al.*, 2007). The new H22Kα mutant strain showed the PS− phenotype (Table 1). *Synechocystis* cells were grown at 30°C under a light intensity of 25–30 μmol photons m^{-2} s^{-1} and continuous bubbling with sterile, humidified air in BG-11 medium (photoautotrophic growth) or BG-11 medium supplemented with 5 mM glucose and 10 μM DCMU (photoheterotrophic growth). Cultures in the exponential growth phase (OD_{730}: 0.6–1.0) were harvested and used for Chl fluorescence measurements and functional analysis.

Generation of H22α and H22β Cyt b_{559} autotrophic transformant mutants by the antenna attenuation method

The pCB(ΔcpcC1C2) km^R and pCK(ΔcpcBAC1C2) km^R plasmids used to delete the corresponding PC rod-forming protein components were constructed as described previously (Ughy & Ajlani, 2004; Thomas *et al.*, 2006). Both plasmids were transformed into H22Yα and H22Cβ Cyt b_{559} mutant cells (Hung *et al.*, 2007). When colonies of transformants appeared on solid agar plates containing the antibiotics erythromycin (Em, 2.5 μg ml^{-1}) and kanamycin (Km, 20 μg ml^{-1}), the colonies were immediately re-streaked and maintained on solid agar plates containing Em (2.5 μg ml^{-1}) only.

Measuring photosynthetic oxygen evolution

Steady-state rates of oxygen evolution in cells were measured using a Clark-type oxygen electrode (Hansatech, Norfolk, UK) fitted with a water-jacketed cell. A cell suspension containing 10 μg Chl was held at 25°C in a stirred, water-jacketed cell. Potassium ferricyanide and 2,6-dichloro-*p*-benzoquinone were added to the samples as artificial electron acceptors (final concentration 2 mM) to a total volume of 1 ml (Huang *et al.*, 2016).

Measuring Chl*a* fluorescence at 295 K

Chl*a* fluorescence measurements at 295 K were performed with a Dual PAM (pulse-amplitude-modulation) fluorometer (Walz, Effeltrich, Germany). A cell suspension containing 16 μg Chl was diluted in PSII content buffer (50 mM MES-NaOH, 25

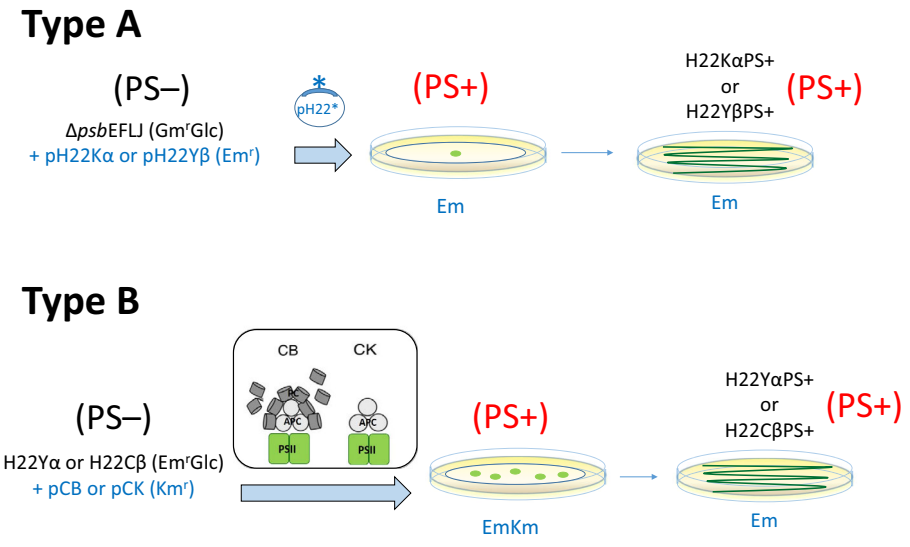

Fig. 1 Procedures for generation of Type A (H22KαPS+ and H22YβPS+) and Type B (H22YαPS+ and H22CβPS+) Cyt b_{559} autotrophic transformants.

© 2021 The Authors
New Phytologist © 2021 New Phytologist Foundation

Table 1 General properties of two distinct types of Cyt b_{559} autotrophic transformants.

Strains	PS growth	Oxygen evolution (% of wild-type)[a]	PSII content (% of wild-type)[b]	References
Wild-type	+	100 ± 6	100 ± 2	This study
Spontaneously generated autotrophic transformants (Type A)				
H22KαPS+	+	84 ± 11	81 ± 16	This study
H22YβPS+	+	41 ± 13	79 ± 19	This study
H22Kα	–	9 ± 1	28 ± 0	This study
H22Yβ	–	~ 0	13 ± 7	Hung *et al.* (2007).
Autotrophic transformants generated through the temporary antenna attenuation method (Type B)				
H22YαPS+	+	54 ± 9	102 ± 12	This study
H22CβPS+	+	23 ± 7	46 ± 10	This study
H22Yα	–	~ 0	17 ± 3	Hung *et al.* (2007)
H22Cβ	–	~ 0	13 ± 5	Hung *et al.* (2007)

[a]Measured as a steady-state rate of oxygen evolution in cells using a Clark-type oxygen electrode in the presence of dichlorobenzoquinone and ferricyanide.
[b]Measured as variable fluorescence in the presence of DCMU and hydroxylamine.

mM $CaCl_2$, 10 mM NaCl, pH 6.5) to a total volume of 1.6 ml and held in a stirred, water-jacketed cell. The relative PSII content of cells on a Chl basis was estimated based on the total yield of variable Chl*a* fluorescence ($F_m - F_0$) measured in the presence of DCMU and hydroxylamine, according to Chu *et al.* (1994). To measure time-dependent flash-induced transients of fluorescence yield, WT or mutant cells were dark-adapted for 5 min. A modulated nonactinic measuring beam (1.6 kHz) was then turned on to obtain the minimal fluorescence value, F_0. Multiple turnover flashes were applied to obtain the fluorescence level of F_m, (maximal fluorescence in the dark) and F'_m (maximal fluorescence in the light). The stable level of fluorescence (F_s) was determined in the presence or absence of red actinic light.

77 K fluorescence measurements

77 K fluorescence emission spectra were recorded with a fluorescence spectrometer (FP-8300; Jasco, Tokyo, Japan) with two different excitation wavelengths: 435 nm to excite Chl*a* (excitation bandwidth 2.5 nm, emission bandwidth 1 nm) and 580 nm to excite the phycobilisomes (excitation bandwidth 2.5 nm, emission bandwidth 1 nm) (Chu *et al.*, 2012; Chiu *et al.*, 2013). All cell suspension samples contained 10 μg Chl ml^{-1}.

DNA-seq library construction and whole-genome sequencing

An amount of 200 ml cells was collected by centrifugation (6000 ***g*** for 10 min) in 250 ml centrifuge bottles. The pellets were frozen in liquid nitrogen and the cell walls were immediately broken in liquid nitrogen using a mortar and pestle. Genomic DNA was extracted and purified from the samples using a DNeasy plant maxi kit (Qiagen). For Illumina sequencing, a paired-end sequencing library was prepared with the KAPA LTP library preparation kit (Roche). The concentrations of the libraries were determined with the Qubit Fluorometer (Invitrogen), and their profiles were determined using a Fragment Analyzer High Sensitivity NGS fragment kit (Agilent, Santa Clara, CA, USA). The molar concentrations of the libraries were derived using qPCR normalisation with a KAPA NGS Library qPCR kit. The prepared libraries were pooled for paired-end sequencing on the Illumina HiSeq 2500 platform at Yourgene Bioscience Co. (New Taipei City, Taiwan) with 125-bp paired-end sequencing reads. DNA-seq reads were mapped to the *Synechocystis* genome using Bowtie2 and Blat. Whole-genome shotgun sequencing involved the PacBio Sequel platform (Pacific Biosciences, Menlo Park, CA, USA). One gel-plus (20 kb) library and one SMRT cell were used. The average read length was 7.1–7.6 kb and the coverage was 43–95%. *De novo* genome assembly involved using the Hierarchical Genome Assembly Process (HGAP) assembler v.4 (Chin *et al.*, 2013).

Southern blot analysis

Southern blot analysis was performed with a DIG High Prime DNA Labeling and Detection Starter Kit I (Roche) according to the manufacturer's instructions. Briefly, genomic DNA (2 μg) was digested with *Kpn*I and *Bsg*I enzymes. pAC559EM (5 ng), used as a positive control, was digested with *Sca*I. The digested DNA was subjected to agarose gel electrophoresis and transferred onto a nylon membrane (Hybond-N+; GE Healthcare, Waukesha, WI, USA). The EFLJ probe was prepared from the pAC559EM plasmid by PCR amplification with primers for B559F (TAGGCGGCTCACAAAATAGT) and for B559R (GG TTTGGGTTTGAATTTCTG).

Droplet digital PCR to detect variation in copy number

Droplet digital PCR (ddPCR) reactions were prepared to contain 10 pg *Alu*-digested genomic DNA and 10 μl of 2× ddPCR Supermix for Probes (Bio-Rad), 900 nM of each primer pair (for the endogenous reference gene and target gene), and 125 nM of each probe; the final volume was adjusted to 20 μl with sterile ultrapure water. The primer pairs and probes are listed in Table S1. The cpcD DNA fragment was used as an endogenous control. 20 μl of each sample and 70 μl of Bio-Rad Droplet Generation Oil were transferred to the respective wells in the cartridges and attached to gaskets. Droplets were generated in a QX200 droplet generator (Bio-Rad). After thermal cycling, the plates were transferred to a QX200 droplet reader (Bio-Rad). The software package provided with the ddPCR system (QuantaSoft 1.7.4.0917; Bio-Rad) was used for data acquisition.

RNA-seq library preparation and next-generation sequencing

Total RNA was isolated from the samples using a miRNeasy mini kit (Qiagen). The quantity and quality of the extracted RNA were determined using a NanoDrop spectrophotometer and an Agilent

© 2021 The Authors
New Phytologist © 2021 New Phytologist Foundation

2100 Bioanalyzer (Agilent). To prepare strand-specific RNA-seq libraries, 5 μg purified RNA was depleted of ribosomal RNA using the Ribo-Zero magnetic kit (Bacteria; Epicentre, Madison, WI, USA) following the manufacturer's instructions. RNA-seq libraries were prepared with the Illumina TruSeq stranded mRNA sample preparation kit (Illumina). The libraries were pooled for paired-end sequencing on the Illumina HiSeq 2500 platform with 125-bp paired-end sequencing reads. Sequencing reads were pre-processed for transcriptomic data analysis using the FASTX Toolkit (v.0.0.13) to remove low-quality bases and reads < 20 bp. After removing reads that mapped to noncoding RNA sequences with BOWTIE v.2.0.0 with default settings, the remaining qualified reads were mapped to the *Synechocystis* genome using BOWTIE with default parameters. Gene expression levels were calculated with the standard reads per kilobase of gene per million mapped reads (RPKM) method. Genes with two-fold or greater changes in expression vs the control in both biological replicates were considered differentially regulated genes.

cDNA synthesis and quantitative real-time PCR

First-strand cDNA was synthesised from 1.5 μg purified RNA using the SuperScript III First-Strand Synthesis System (Invitrogen) with random hexamers. The constitutively expressed gene *rnpB* was used as a reference. The resulting cDNA was amplified with gene-specific forward and reverse DNA oligonucleotides, as listed in Table S2. Quantitative RT-PCR was performed on an ABI 7500 Real-Time PCR System (Applied Biosystems, Waltham, MA, USA), and the amount of cDNA was detected with SYBR Green dye.

Radioactive labelling of proteins *in vivo*

Radioactive pulse labelling of cells was performed at 30°C for 30 min under 500 μmol photons m^{-2} s^{-1} of illumination using a mixture of [^{35}S]Met and [^{35}S]Cys (Hartmann Analytic Gmbh, Braunschweig, Germany) as described (Dobáková *et al.*, 2007). For each strain, labelling was performed using the same number of cells corresponding to 75 μg Chl in the WT, which were re-suspended in 250 μl BG-11.

Preparation of cellular membranes

Cells in the exponential growth phase (100 ml) were pelleted, washed, and re-suspended in buffer B (25 mM MES/NaOH, pH 6.5, 10 mM $CaCl_2$, 10 mM $MgCl_2$, 25% glycerol (v/v)). The cells were broken mechanically in a Mini-Beadbeater (BioSpec, Bartlesville, OK, USA) using balotina beads. The membrane and soluble protein fractions were separated by high-speed centrifugation (47 000 ***g***, 20 min). The pelleted membranes were washed and re-suspended in buffer B.

Two-dimensional PAGE analysis of membrane proteins and immunoblotting

Two-dimensional analysis of membrane proteins was performed using a combination of clear native (CN) PAGE in a 4% to 12% gradient gel and SDS-PAGE in a 12% to 20% gradient gel containing 7 M urea (2D CN/SDS-PAGE) (Kiss *et al.*, 2019). For immunoblotting, the gels were stained with SYPRO Orange (Sigma-Aldrich); proteins from the gel were transferred onto a PVDF membrane that was incubated with a specific primary antibody, followed by a secondary antibody conjugated with horseradish peroxidase (Sigma-Aldrich). The primary antibodies against D1, D2, CP43, PsbE and PsbF used in this study, which were prepared in rabbits, were described previously (Komenda *et al.*, 2008). Two-dimensional gels with radioactively labelled proteins were stained with Coomassie Brilliant Blue, photographed, dried, exposed to a phosphorimager plate (GE Healthcare) overnight, and scanned using a Storm 860 phosphorimager (GE Healthcare).

Results

Generation of a new type of autotrophic Cyt b_{559} transformant by the antenna attenuation method

To characterise the changes responsible for the conversion of the nonautotrophic axial histidine Cyt b_{559} mutants into autotrophic strains, we analysed two different types of these autotrophic transformants. Type A autotrophic transformants, in which the His22 residues in PsbE and PsbF were replaced by Lys and Tyr, were designated H22KαPS+ and H22YβPS+, respectively; these transformants were previously isolated by transforming a strain lacking *psbEFLJ* with the corresponding plasmid containing the mutated gene, following by segregation on glucose-free agar plates, as described previously (Hung *et al.*, 2007) (Fig. 1). Type B autotrophic transformants were prepared with the antenna attenuation method applied to the original nonautotrophic Cyt b_{559} histidine mutants H22Yα and H22Cβ (Hung *et al.*, 2007). This method is based on the parallel induction of autotrophic transformants and the site-directed removal of phycobilisome rod linker proteins LR33 and LR30 (ΔcpcC1C2, abbreviated CB), resulting in a strain lacking two of three phycocyanin (PC) hexamers per rod (Ughy & Ajlani, 2004; Hung *et al.*, 2010); or (2) all PC rod-forming subunits, resulting in mutant cells lacking PC and containing only the allophycocyanin (APC) core (Ughy & Ajlani, 2004; Thomas *et al.*, 2006) (Fig. 1). During this process, the decrease in antenna size may provide photoprotection or better resource allocation to autotrophic transformants, therefore leading to their more efficient generation and better survival.

Without this antenna attenuation step, no autotrophic transformant/pseudorevertants were obtained. However, once autotrophic transformants were generated, the reduced antenna size became deleterious for autotrophic proliferation and, in the absence of selection antibiotics (Km), they recovered the capacity to assemble a full phycobilisome (Table S3). When the autotrophic transformants were further propagated on agar plates containing Km, they lost their ability to undergo photosynthetic growth and died. We generated a number of these autotrophic transformants but, for the purpose of this study, as representatives of Type B autotrophic transformants, we used only two strains with the His22 residues of PsbE and PsbF replaced by Tyr

© 2021 The Authors
New Phytologist © 2021 New Phytologist Foundation

and Cys residues, from this point forwards designated as H22YαPS+ and H22CβPS+, respectively.

Growth, oxygen evolution activity and PSII contents of mutant cells

The growth characteristics, light-saturated oxygen evolution activity, and PSII content of the representative mutant strains are listed in Table 1. All autotrophic transformants were able to grow photoautotrophically and assemble appreciable amounts of PSII complexes, as judged from their oxygen-evolving activities and quantification of PSII levels via measurement of variable fluorescence in the presence of DCMU and hydroxylamine (Chu *et al.*, 1994). Among the autotrophic transformants, H22KαPS+ cells showed the highest oxygen evolution activity (*c.* 84% compared with WT), whereas H22CβPS+ showed the lowest oxygen evolution activity (*c.* 23% compared with WT). By contrast, all corresponding Cyt b_{559} mutant strains (H22Kα, H22Yα, H22Yβ, and H22Cβ) failed to grow photoautotrophically, showed little or no oxygen evolution activity, and could not accumulate appreciable amounts of PSII core complexes (Table 1). Under our experimental growth conditions for photoautotrophic growth (light intensity of 30 μmol photons m^{-2} s^{-1}), the doubling times for WT, H22KαPS+, H22YβPS+, H22YαPS+ and H22CβPS+ cells were *c.* 13, 14, 26 (Hung *et al.*, 2007), 23 and 53 h, respectively (Fig. S1).

Maximum quantum yield of PSII photochemistry (F_v/F_m) was recovered in Cyt b_{559} autotrophic transformants

Compared with WT and Cyt b_{559} mutant cells, autotrophic transformant cells showed distinct time-dependent, flash-induced transient fluorescence yields in the presence and absence of actinic light (Fig. 2a). WT cells had a lower F_0 value (*c.* 0.13) and higher F_v/F_m value (*c.* 0.43) (Fig. 2a, panel i) than the autotrophic transformants, whose F_0 values ranged from 0.15 to 0.24 and F_v/F_m values from 0.41 to 0.15 (Fig. 2a, panels ii–v). By contrast, the corresponding Cyt b_{559} mutant H22Kα and H22Yα strains failed to grow photoautotrophically and had higher F_0 values (0.29 and 0.33, respectively) and much lower F_v/F_m values (*c.* 0.01) (Fig. 2a, panels vi–vii) than the autotrophic transformants. In addition, the maximum fluorescence (F'_m) in Cyt b_{559} autotrophic transformant cells significantly increased during illumination with actinic light and decreased after this treatment. However, for WT, the F'_m values were approximately the same before, during and after actinic light illumination. The changes in maximal fluorescence yield elicited by actinic light in the autotrophic transformants can be attributed to state transitions (Huang *et al.*, 2018; Calzadilla & Kirilovsky, 2020; and references therein) and to the fluorescence emissions from uncoupled phycobilisomes (Chiu *et al.*, 2013).

Finally, most autotrophic transformants and especially the H22CβPS+ mutant showed decreased steady-state fluorescence below the F_0 level that gradually increased after actinic light illumination was switched off (Fig. 2a, panel v). This result suggests that a fluorescence quencher was induced by the actinic light in a significant fraction of PSII in the autotrophic transformants, especially the H22CβPS+ mutant. This phenomenon has been attributed to back electron flow from dark reduction of the plastoquinone pool to PSII and is typical of acceptor-side photoinhibition (Bondarava *et al.*, 2003; Ohad *et al.*, 2004; Chiu *et al.*, 2013).

77 K fluorescence emission spectra

The top panel of Fig. 2(b) shows the 77 K fluorescence emission spectra for cells excited at 435 nm, a wavelength that Chl molecules preferentially absorb. In the spectra for WT and Cyt b_{559} autotrophic transformant cells, preferential excitation of Chl at 435 nm resulted in three emission peaks: at *c.* 686, *c.* 695, and *c.* 724 nm. The emission peak at *c.* 686 nm originates from CP43 and the peaks at *c.* 695 and *c.* 724 nm originate from functional PSII and PSI reaction centres, respectively (Andrizhiyevskaya *et al.*, 2005; Boehm *et al.*, 2011; Lamb *et al.*, 2018; Calzadilla & Kirilovsky, 2020; and references therein). Therefore, the increased emission peaks at *c.* 695 and *c.* 686 nm in the spectra for H22YαPS+, H22KαPS+, and H22YβPS+ may indicate that the ratio of PSII to PSI and the level of unassembled CP43 in these autotrophic transformants were higher than in the WT. In addition, the low emission peaks at *c.* 695 nm for the H22CβPS+, H22Kα and H22Yα mutants were associated with lower PSII content in these mutants in comparison with WT and the other mutants (Fig. 2a).

The bottom panel of Fig. 2(b) shows the 77 K fluorescence emission spectra recorded from cells excited at 580 nm, a wavelength that is preferentially absorbed by phycobilin pigments. The WT strain showed emission peaks with maxima at *c.* 664 nm (from APC), *c.* 690 nm (from PSII), and *c.* 723 nm (from PSI) (Ughy & Ajlani, 2004; Hung *et al.*, 2007, 2010). In the spectra for the Cyt b_{559} autotrophic transformants as well as H22Kα and H22Yα mutants, the emission peaks were strongly enhanced and shifted to *c.* 686 nm. The emission peaks at *c.* 686 nm mainly originates from terminal phycobilin emitters (Lamb *et al.*, 2018; Calzadilla & Kirilovsky, 2020). Therefore, the enhanced emission peaks at 686 nm in these mutant strains indicate that the energy transfer from phycobilisomes to PSII reaction centres was significantly inhibited or uncoupled in these cells.

The genomes of the Cyt b_{559} autotrophic transformants carry tandem repeats containing the *psbEFLJ* operon

To identify the possible second-site mutation(s) in the genomes of the Cyt b_{559} autotrophic transformants, we sequenced their entire genomes and mapped the next-generation sequencing data to the *Synechocystis* genomic sequence. These autotrophic transformants did not carry significant second-site mutation(s), but all had > 5–15 times increased read coverage in the regions containing *psbEFLJ* operons in their genomes (Fig. 3a). These results suggest that the autotrophic transformants carry high copy numbers of DNA segments containing the *psbEFLJ* operon. The multiplication units in the H22YαPS+ and H22CβPS+ (Type B) strains were *c.* 24 and 96 kb, respectively.

© 2021 The Authors
New Phytologist © 2021 New Phytologist Foundation

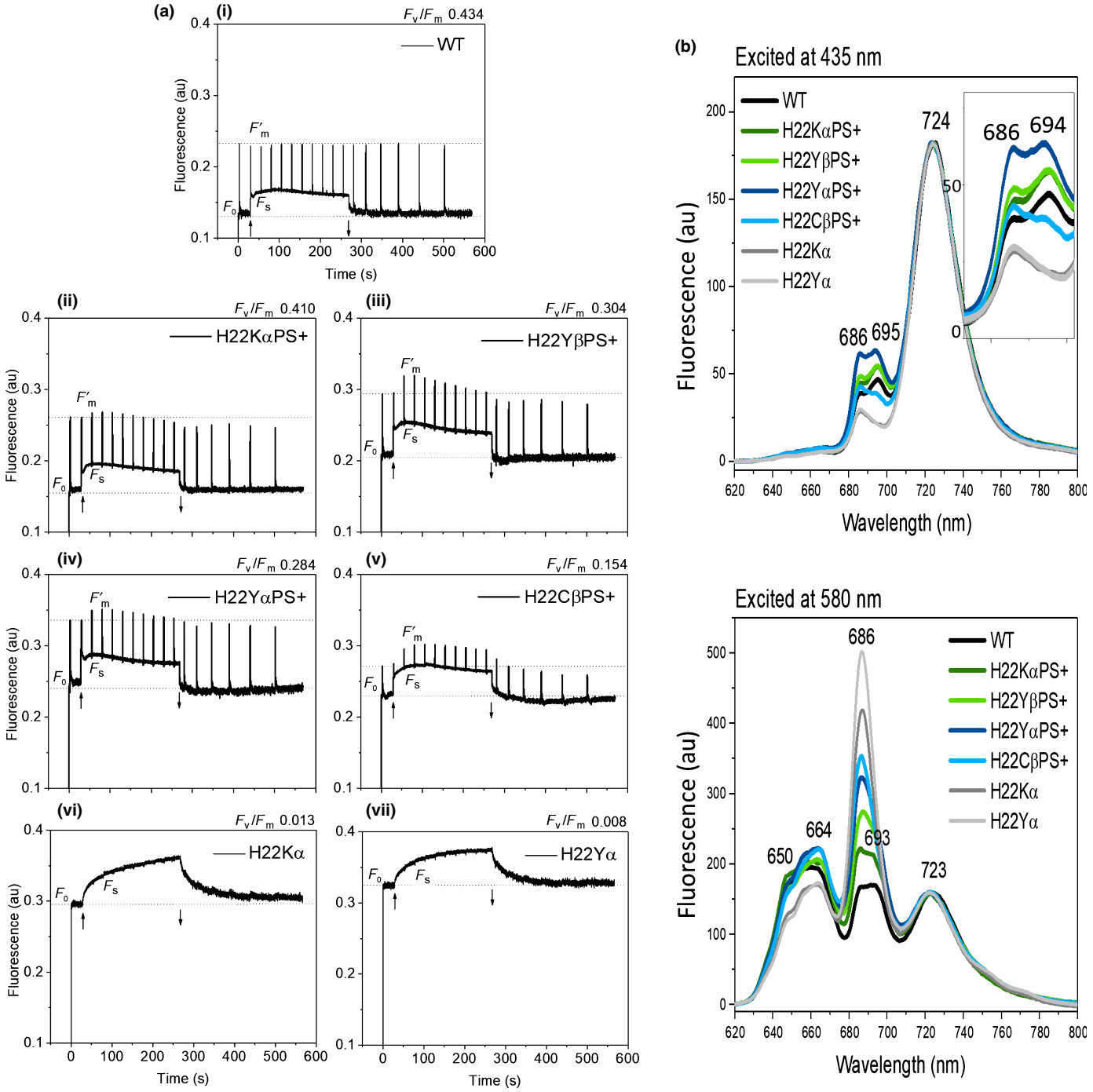

Fig. 2 Photosynthetic characterisation of WT and Cyt b_{559} mutant cells. (a) Time-dependent flash-induced transients of PSII fluorescence yield of WT and Cyt b_{559} mutant cells with and without red actinic light. The light intensity of red actinic light was *c.* 40 μmol photons m^{-2} s^{-1}. Up arrow (↑) indicates actinic light on. Down arrow (↓) indicates actinic light off. (b) 77 K fluorescence emission spectra from WT and Cyt b_{559} mutant cells. Spectra were normalised to emission of PS I. au, arbitrary units.

The copy number of the *psbEFLJ* operon in the autotrophic transformants varies under different growth conditions

We performed ddPCR to determine the copy number variation of *psbEFLJ* in the transformants by comparing the ratios of the *psbEFLJ* gene products with the reference *cpcD* products. The high copy number of the *psbEFLJ* genes was verified in all autotrophic transformants (Fig. 3b). By contrast, all corresponding Cyt b_{559} mutant strains (H22Kα, H22Yβ, H22Yα, and H22Cβ) failed to grow photoautotrophically, showed a single copy number of *psbEFLJ* genes and did not carry the pUC119 plasmid sequence in their genomes. In addition, we used ddPCR analysis to characterise the stability of the number of *psbEFLJ* operon repeats in these strains under photoheterotrophic

© 2021 The Authors
New Phytologist © 2021 New Phytologist Foundation

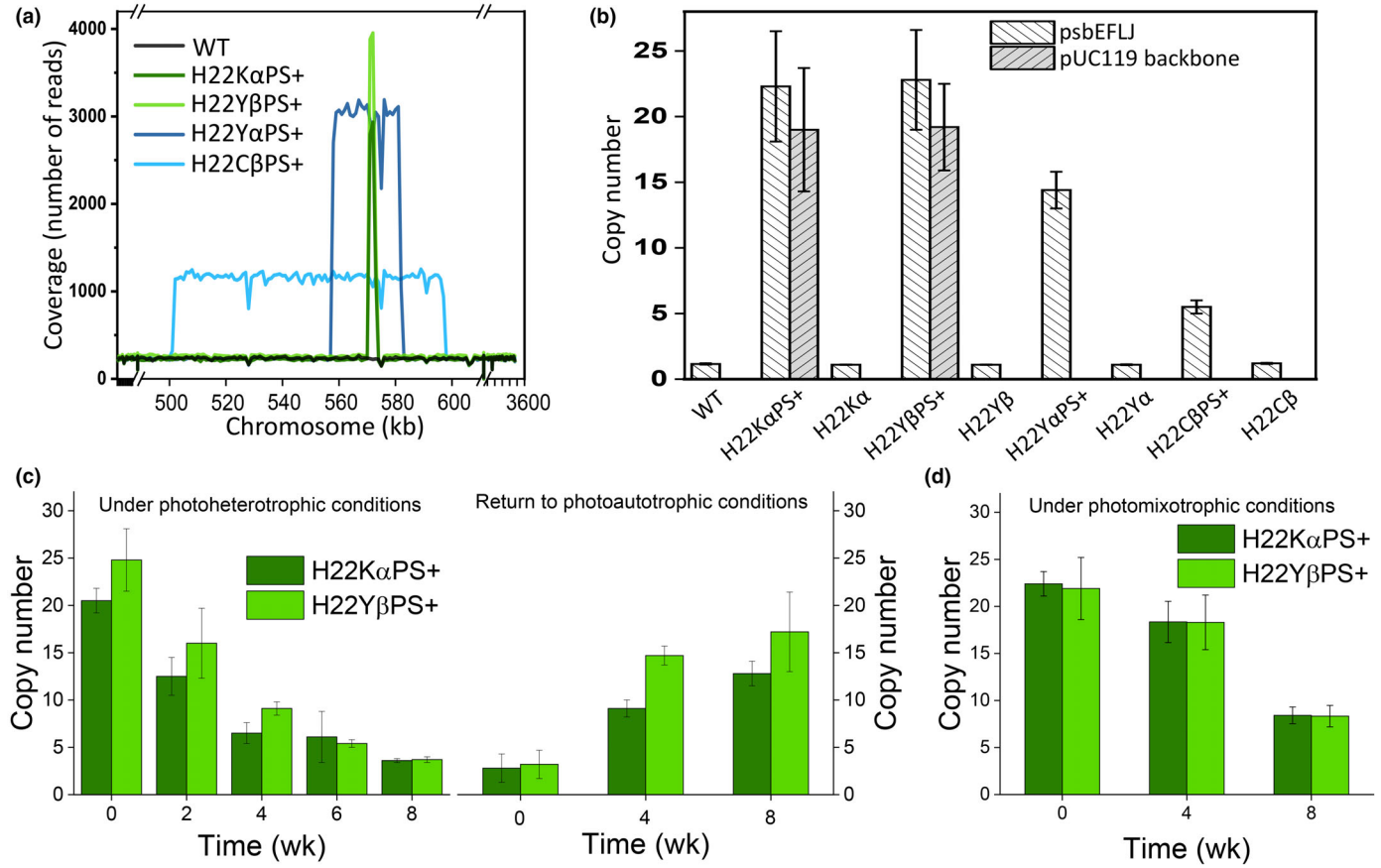

Fig. 3 Genomic analysis of autotrophic transformant cells. (a) Copy number, size and location of repeat elements in autotrophic transformant cells. (b) Copy number variation of *psbEFLJ* and pUC119 backbone in WT and autotrophic transformants by droplet digital PCR (ddPCR) ($n = 3$). (c) ddPCR analysis of the time course of copy number variation of *psbEFLJ* in autotrophic transformants grown under photoheterotrophic conditions and then returned to photoautotrophic conditions ($n = 2$). (d) ddPCR analysis of the time course of copy number variation of *psbEFLJ* in autotrophic transformants grown under photomixotrophic conditions ($n = 2$). Data are the mean ± SD.

conditions (plus the PSII inhibitor DCMU and glucose). Under these conditions, the number of repeats in the Type A transformants gradually decreased from *c.* 20 to 3 copies within 8 wk of photoheterotrophic growth (Fig. 3c). However, when the cultures were shifted back to photoautotrophic growth conditions, the copy numbers of the *psbEFLJ* genes gradually increased and returned to the original levels. Furthermore, under photomixotrophic conditions (with glucose), the number of repeats in the Type A transformants gradually decreased from *c.* 20 to *c.* 8 copies within 8 wk (Fig. 3d). The results suggest that the high copy number of the *psbEFLJ* genes is required for photoautotrophic growth of the autotrophic transformants.

Repeats of the *psbEFLJ* operon are located on chromosomes of the autotrophic transformants

To examine whether the *psbEFLJ* operon repeats were located on chromosomes or plasmids of the autotrophic transformants, we performed Southern blot analysis. We used the restriction enzymes *Kpn*I and *Bsg*I to digest the chromosome because their restriction sites are located outside of the *psbEFLJ* operon (Fig. 4a). When we used a *psbEFLJ* probe to identify fragments containing the *psbEFLJ* operon, WT and the Type B transformants showed one hybridisation band of *c.* 5.3 kb (Fig. 4b). By contrast, the hybridisation bands in the Type A autotrophic transformants were much larger (> 23 kb). These results confirm that the mutant plasmids were integrated into (and amplified in) the chromosomes of the Type A transformants. In addition, although the hybridisation bands in the Type B transformants were the same size as for the WT, the bands were more intense in the transformants compared with WT, which is consistent with the amplification of the *psbEFLJ* operon.

Sequence analysis of the amplified chromosome segments in autotrophic transformants

All autotrophic transformants examined retained the heme-ligand mutations, as revealed by whole-genome sequencing and PCR Sanger sequencing (Table S4). In addition, the multiplication units in all autotrophic transformants were direct tandem repeats. The repeats in H22KαPS+ transformants exactly matched the size of the pAC559Em plasmid (*c.* 7 kb). In H22YβPS+ transformants, about half of repeats had the same size as the pAC559Em plasmid and the others had a reduced size

© 2021 The Authors
New Phytologist © 2021 New Phytologist Foundation

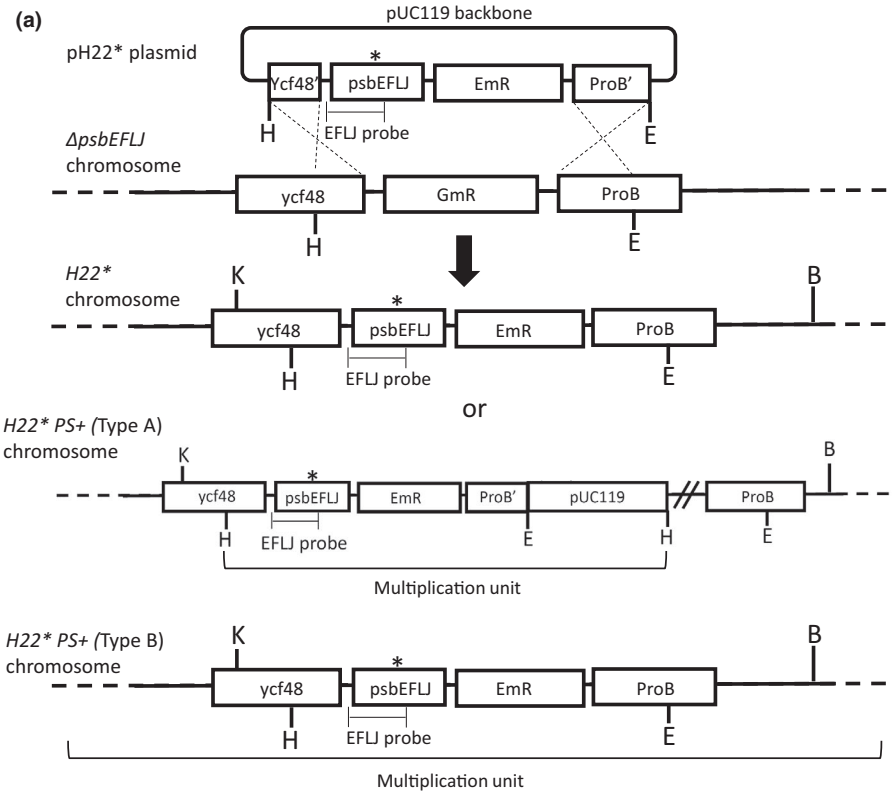

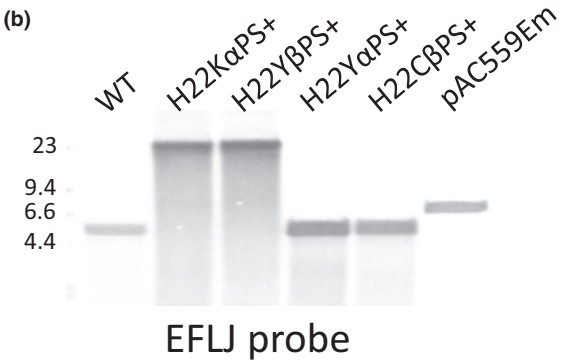

Fig. 4 Schematic representation of chromosome structure (a) and Southern blot analysis (b) of WT and Cyt b_{559} mutants. The mutation site of H22Hα or H22β is indicated as a star (*) in (a). Restriction enzyme site: H, *Hin*dIII; E, *Eco*RI; K, *Kpn*I; B, *Bsg*I. Genomic DNA was digested with *Kpn*I and *Bsg*I. pAC559Em plasmids were a positive control. The probe used in (b) was the EFLJ probe.

due to deletion of EmR (coding for Em resistance gene) (Fig. S2). We also analysed the border and junction sequences flanking the multiplication units. No sequences were inserted or deleted in junctions between the repeats. However, the border sequences of the multiplication units in the Type B transformants all differed (Fig. 5a). A hexanucleotide sequence (5′-TCCATT-3′) was present in border sequences of the multiplication units in H22YαPS+ and H22CβPS+. In addition, the sequence 5′-TTCGTT-3′ was present in both the 5′-end and 3′-end border sequences as well as in new junction sequences between the individual repeats within the multiplication units in H22CβPS+ but was absent in all other autotrophic transformants. Furthermore, the Type B autotrophic transformants all had a very short (1–5 nucleotides) homologous junction sequence flanking the multiplication units (Fig. 5b). The mechanism of tandem gene multiplication in the Type B transformant is likely to be initiated by RecA-independent illegitimate recombination that utilises very short homologous sequences (Fig. 5c) (Andersson & Hughes, 2009; Reams & Roth, 2015).

The *psbEFLJ* operon and several photosynthesis-related genes were differentially expressed in the autotrophic transformants

The transcript levels of *psbEFLJ* genes were 16-fold to 27-fold and 6-fold to 23-fold higher in the Type A and Type B autotrophic transformants, respectively, compared with WT, as revealed by RNA-seq (Table 2) and quantitative RT-PCR (Fig. 6). The other photosynthesis-related genes that were significantly upregulated (2-fold to 7-fold) in most autotrophic transformants vs WT included *psbD2* (*slr0927*, the gene for D2), *hliB* (*ssr2595*, the gene for high light-inducible HliB stress protein (He *et al.*,

© 2021 The Authors
New Phytologist © 2021 New Phytologist Foundation

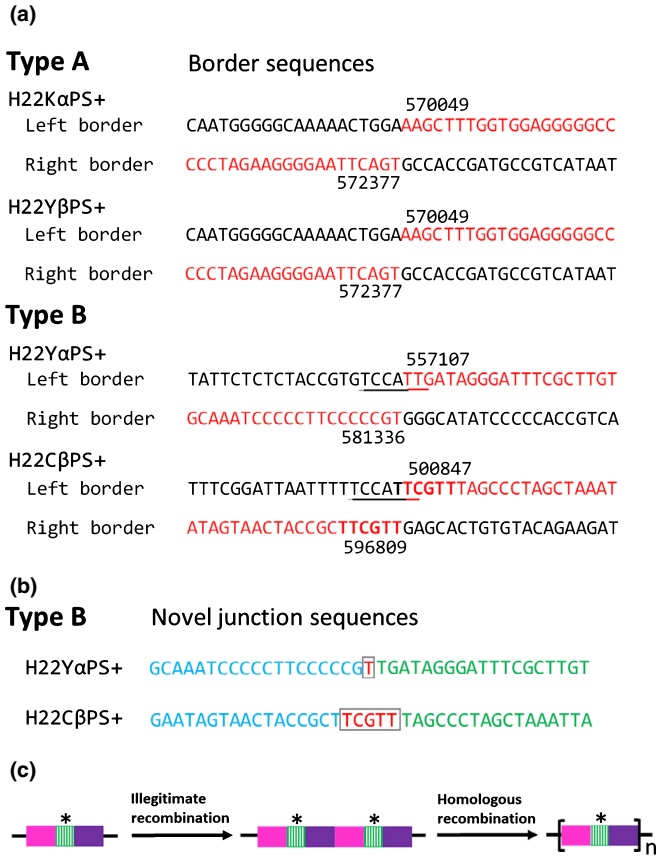

Fig. 5 Analysis of the sequences at the borders and junctions of the amplified chromosome fragments in autotrophic transformants. (a) Border sequences: two short regions of homologous sequences (5′-TCCATT-3′ and 5′-TTCGTT-3′) are shown as underline and bold type, respectively. (b) Novel junction sequences: the presence of very short (1–5 nucleotides) homologous junction sequences in Type B autotrophic transformants are indicated in boxes and red colour. (c) A model for tandem gene amplification of chromosome segments containing the *psbEFLJ* operon (marked with an asterisk) in Type B autotrophic transformants.

2001)), *ftsH3* (*slr1604*, the gene for FtsH3 protease (Komenda *et al.*, 2006)) and *bicA* (*sll0834*, the gene for a low-affinity, high-flux Na^+-dependent SulP type bicarbonate transporter (Wang *et al.*, 2019)). The significantly downregulated photosynthesis-related genes in these transformants included *sll1471* (*cpcG2*, the gene for a phycobilisome linker (Kondo *et al.*, 2007)), *cmpA/B* (*slr0040/slr0041*), *sbtA/B* (*slr1512/1513*), *cupA* (*sll1734*) and *ndhD3* (*sll1733*) (involved in inorganic carbon transport systems (Omata *et al.*, 1999; Zhang *et al.*, 2004)), *sigE* (*sll1689*, encodes an RNA polymerase sigma factor involved in regulating sugar catabolism and photosystem-related genes (Tokumaru *et al.*, 2018)) and *sll0450* (*norB*, the gene for a quinol-dependent single-subunit nitric oxide reductase (Busch *et al.*, 2002)) (Table 3). Furthermore, genes within the tandemly amplified segments in the Type B transformants (e.g. from region SGL_RS04470 to SGL_RS04590 in H22YαPS+) were all upregulated. Therefore, the high copy numbers of these genes resulted in high transcript levels (Table S5).

Analysis of membrane protein complexes reveals differences among WT, Cyt b_{559} mutants and the corresponding autotrophic transformants

To evaluate the impact of the Cyt b_{559} mutations and both types of pseudoreversions on the membrane composition and (especially) content and assembly state of PSII complexes, we analysed membranes of WT and the H22Kα, H22Yβ and H22Yα mutants and the corresponding autotrophic transformants H22KαPS+ and H22YβPS+ (Type A) and H22YαPS+ (Type B) using a combination of CN and SDS gel electrophoresis followed by protein immunodetection. CN-PAGE analysis (Fig. 7) clearly documented the differences in PSI and PSII complex contents between the Cyt b_{559} mutants and the corresponding autotrophic transformants. As judged from the Chl fluorescence scan of the gel, all Cyt b_{559} mutants were strongly depleted in the assembled dimeric and monomeric PSII core complexes (PSII(2) and PSII (1)), but they contained a highly fluorescent band in a region containing small proteins most probably belonging to the unassembled PSII antennae (see results of 2D immunoblotting described below). In the autotrophic transformants, the levels of PSII(2) and PSII(1) markedly increased and were higher in the H22KαPS+ strain vs the two other autotrophic transformants; these findings are in agreement with the PSII contents determined by variable fluorescence measurements (Table 1). Furthermore, the increased PSII levels in the autotrophic transformants were accompanied by the depletion of unassembled antenna proteins. The contents of PSI complexes in the strains, especially the trimer, were proportional to the levels of PSII complexes, confirming the notion that PSI levels depend on the activity and accumulation of PSII complexes (Kiss *et al.*, 2019).

To confirm the identity of the PSII complexes observed in the CN gel and to obtain a more complete information about their composition (focusing on the presence of mutated PsbE and PsbF subunits of Cyt b_{559}), we analysed the complexes that were separated by CN-PAGE by SDS-PAGE and immunoblotting in the second dimension (Figs 8, 9, S3). SYPRO staining and immunodetection with antibodies that specifically recognise D1, D2 and CP43 confirmed both the identity of the separated fluorescent complexes as PSII(2) and PSII(1) and the differences in their levels between the Cyt b_{559} mutants and the corresponding autotrophic transformants. The PSII complexes contained all large proteins examined as well as both the PsbE and PsbF subunits. SYPRO staining and immunodetection confirmed the presence of the CP47 and CP43 antennae in the fluorescence band in the region containing unassembled proteins in the mutants (on 2D stained gels, indicated by arrows).

A more detailed look at individual protein contents showed that the Cyt b_{559} mutants contained low levels of unassembled D1 protein (indicated by an arrow) but lacked any unassembled D2. Because we previously showed that the absence of PSII in the strain lacking the *psbEFLJ* operon is related to the inhibition of D2 synthesis (Komenda *et al.*, 2004), the depletion of PSII in the mutant is most likely to be due to the lack of functional PsbE and PsbF. To verify this hypothesis, we radioactively labelled H22K mutant cells and the autotrophic transformant

© 2021 The Authors
New Phytologist © 2021 New Phytologist Foundation

Table 2 A list of common upregulated photosynthesis-related genes in autotrophic transformant cells.

Gene ID	Symbol	Fold change related to the level in WT				Description
		H22KαPS+	H22YβPS+	H22YαPS+	H22CβPS+	
Photosystem II						
slr2034	*ycf48*	2.2	2.7	12.8	5.9	PS II assembly factor Ycf48
ssr3451	*psbE*	16.4	25.0	21.3	5.5	Cyt b_{559} subunit alpha
smr0006	*psbF*	15.6	23.3	21.0	5.6	Cyt b_{559} subunit beta
smr0007	*psbL*	16.0	25.9	22.8	7.9	PsbL
smr0008	*psbJ*	15.2	26.5	21.7	7.0	PsbJ
sll0851	*psbC*	1.5	2.5	2.7	2.6	CP43
sll0849	*psbD1*	1.7	2.8	2.9	2.4	D2 protein
slr0927	*psbD2*	2.3	5.9	5.0	4.9	D2 protein
Photoprotection						
slr1604	*ftsH3*	1.7	3.1	2.9	5.1	ATP-dependent metallopeptidase
ssr2595	*hliB*	2.7	3.3	2.5	3.2	High light-inducible protein
slr0228	*ftsH2*	1.4	2.0	1.9	2.7	ATP-dependent metalloprotease
Transporters						
sll0834	*bicA*	1.7	2.8	6.4	3.0	Bicarbonate transporter BicA

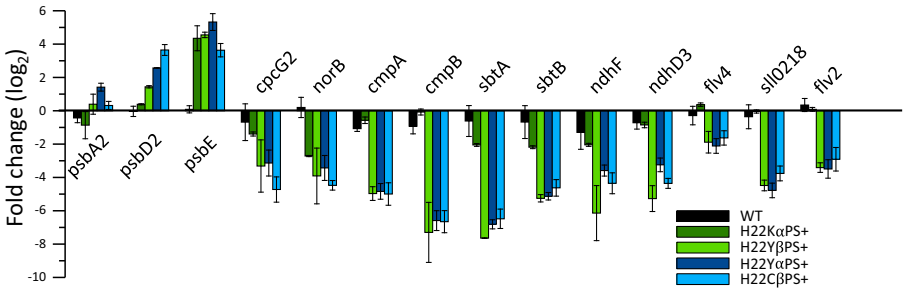

Fig. 6 Changes in transcript abundance in WT and autotrophic transformants under photoautotrophic growth conditions using real-time PCR. The primer pairs are described in Table S5. The transcript level of *rnpB* was used as a reference. Data are the mean ± SD from three independent cultivation experiments.

H22KαPS+ and compared the patterns of their labelled membrane proteins using 2D CN/SDS-PAGE combined with autoradiography (Fig. 10). Notably, in both strains, most D1 protein (in all three forms: pD1 precursor, iD1 intermediate, and D1 mature protein (indicated by a triple arrow)) was identified in the region of unassembled proteins together with labelled CP43 and CP47. However, unlike the Cyt b_{559} mutant, the autotrophic transformant contained some labelled D2 protein in PSII(1) and PSII(2). These results support the notion that insufficient biosynthesis of D2 due to a deficiency of PsbE and PsbF is the reason for the depletion of PSII and the lack of autotrophic growth of the mutants with defects in the axial ligands of Cyt b_{559}.

Discussion

In the current study, regardless of how the autotrophic transformants were obtained, whole-genome sequencing revealed that all four strains lacked true second-site mutations, but all contained 5-fold to 15-fold tandem repeats of the chromosomal regions containing the *psbEFLJ* operon with the original Cyt b_{559} mutation (Fig. 3a). The sizes of the tandem repeat units depended on the procedure used to obtain these autotrophic transformants. Type A transformants such as H22KαPS+ and H22YβPS+, containing *c.* 7-kb repeat units, were generated during the selection of the *psbEFLJ*-less strain for autotrophy using a plasmid containing the mutated *psbE/F* gene. The size of the repeat units present in these strains corresponded well to the size of the *psbEFLJ* operon, resistance cassette, flanking regions comprising parts of the *ycf48* and *proB* genes, and the rest of the plasmid. There were no additional nucleotide sequences at the border of the whole multiplication unit or at the internal junction points between the individual repeats. This type of tandem multiplication probably involved integration of the entire mutant plasmid into the genome, followed by its tandem multiplication via rolling cycle replication or other mechanisms (Andersson & Hughes, 2009; Reams & Roth, 2015). In H22YβPS+ transformants, about half of the repeats had the reduced size due to deletion of EmR (Fig. S2). This could be a secondary event occurring during tandem multiplication. Notably, an ISY203a transposase gene (*slr2036*) is located downstream of the *psbEFLJ* operon, but whether this transposase plays a significant role in the tandem multiplication process is unknown.

By contrast, Type B transformants such as H22CβPS+ contained much larger repeat units (up to 96 kb). The presence of these repeat units points to the internal spontaneous amplification of a large DNA segment. Type B transformants do not contain a common repetitive sequence flanking multiplication units, but all have a very short (1–5 nucleotides) homologous junction sequence flanking its multiplication units. Because the RecA-mediated homologous recombination generally requires lengths

© 2021 The Authors
New Phytologist © 2021 New Phytologist Foundation

Table 3 A list of common downregulated photosynthesis-related genes in autotrophic transformant cells.

Gene ID	Symbol	Fold change related to the level in WT				Description
		H22KαPS+	H22YβPS+	H22YαPS+	H22CβPS+	
Photosynthesis						
sll0219	*flv2*	−1.2	−2.3	−4.0	−3.1	Flavoprotein
sll0218		−1.2	−1.9	−4.6	−2.6	Hypothetical protein
sll0217	*flv4*	1.1	−1.1	−1.5	−2.6	Flavoprotein
sll1471	*cpcG2*	−4.5	−3.8	−40.3	−42.9	Phycobilisome rod-core linker
Inorganic carbon transports						
sll1734	*cupA*	−1.3	−2.4	−2.6	−4.0	CO_2 hydration protein
sll1733	*ndhD3*	−1.4	−2.7	−2.4	−4.2	NADH dehydrogenase subunit
sll1732	*ndhF3*	1.0	−2.6	−1.8	−4.5	NADH dehydrogenase subunit
slr1512	*sbtA*	−1.3	−2.5	−9.6	−9.6	Sodium dependent bicarbonate transporter
slr1513	*sbtB*	−1.1	−1.8	−5.9	−4.8	Hypothetical protein
slr0040	*cmpA*	−1.7	−8.5	−16.9	−19.9	Transporter substrate-binding protein
slr0041	*cmpB*	−1.6	−8.5	−25.5	−13.9	Bicarbonate transporter permease
slr0043	*cmpC*	−1.3	−2.5	−4.5	−3.2	Transporter ATP-binding protein
slr0044	*cmpD*	−1.2	−2.3	−5.7	−5.0	Transporter ATP-binding protein
Metabolism						
sll1689	*sigE*	−1.7	−2.8	−4.1	−4.3	RNA polymerase sigma factor, sigE
sll0450	*norB*	−6.1	−12.1	−25.4	−18.4	Nitric oxide reductase

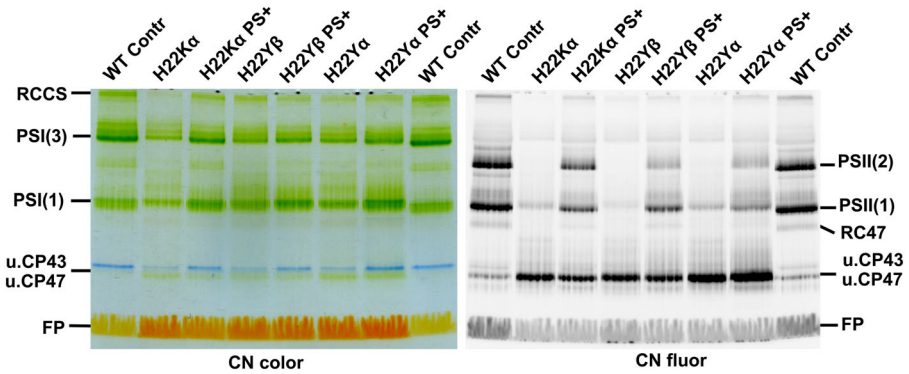

Fig. 7 Analysis of photosynthetic complexes in site-directed mutants of cytochrome b_{559} and corresponding autotrophic transformants of *Synechocystis*. The strains were grown in BG11 containing 5 mM glucose at 40 µmol photons m^{-2} s^{-1}. Designation of complexes: FP, free pigments; PSI(3) and PSI(1), trimeric and monomeric Photosystem I; PSII(2) and PSII(1), dimeric and monomeric PSII core complexes; RCCS, supercomplex of PSI and PSII; RC47, the monomeric PSII core complex lacking CP43; u.CP43 and u.CP47, unassembled PSII antennae. Loading was performed based on the same $OD_{750\ nm}$; in WT, this $OD_{750\ nm}$ corresponded to 4 µg Chl.

of repetitive sequences of at least 20–40 nucleotides (Andersson & Hughes, 2009), the mechanism of tandem multiplications in the Type B transformant may be initiated by illegitimate recombination that utilises a very short homologous sequence and could be further amplified by RecA-mediated homologous recombination (Fig. 5c) (Andersson & Hughes, 2009; Reams & Roth, 2015). Such gene amplifications occur in many organisms, from bacteria to higher eukaryotes, and may play important roles in evolutionary adaptation to selection pressure and stressful environmental conditions (Andersson & Hughes, 2009; Elliott *et al.*, 2013; Reams & Roth, 2015). To our knowledge, this is the first report of targeted tandem gene amplification in cyanobacteria.

One recent study reported the tandem duplication of a large (110-kb) chromosomal segment in a glucose-tolerant substrain (GT-W) of *Synechocystis* (Tichý *et al.*, 2016). This tandemly duplicated large chromosomal segment harbours *c.* 100 genes, including several PSII-related genes (such as *psbA2* and *psb28*) and the gene for Mg-protoporphyrin methylestercyclase. In addition, this chromosomal segment is bordered by two ISY100 transposases, *sll0431* and *sll1397*, which might mediate this tandem multiplication process. The GT-W strain showed aberrant PSII assembly and deficient Chl biosynthesis compared with the PCC strain of *Synechocystis* (Tichý *et al.*, 2016). Notably, tandem multiplication in the genomes of GT-W cells was selected during prolonged growth on glucose and disappeared in cells grown on agar plates under photoautotrophic conditions (Tichý *et al.*, 2016). Similarly, we detected changes in tandem repeat numbers in the autotrophic transformants depending on growth conditions (photoautotrophic vs photoheterotrophic growth).

As revealed by RNA-seq and quantitative RT-PCR, the formation of multiple tandem repeats containing the *psbEFLJ* operon

© 2021 The Authors
New Phytologist © 2021 New Phytologist Foundation

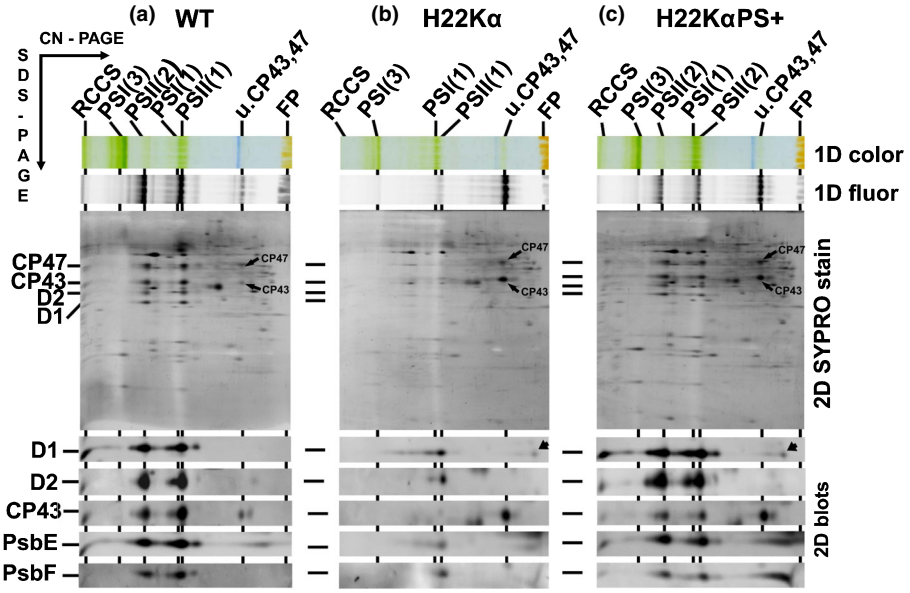

Fig. 8 Two-dimensional PAGE analysis of photosynthetic complexes in (a) WT, (b) the site-directed mutant H22Kα and (c) its corresponding autotrophic transformant H22KαPS+ of *Synechocystis* sp. PCC6803. The strains were grown in BG11 containing 5 mM glucose at 40 μmol photons m^{-2} s^{-1}. Designation of complexes as in Fig. 7. Arrows in the blot designate unassembled D1. Loading was based on the same $OD_{750\ nm}$; in WT, this $OD_{750\ nm}$ corresponded to 4 μg Chl.

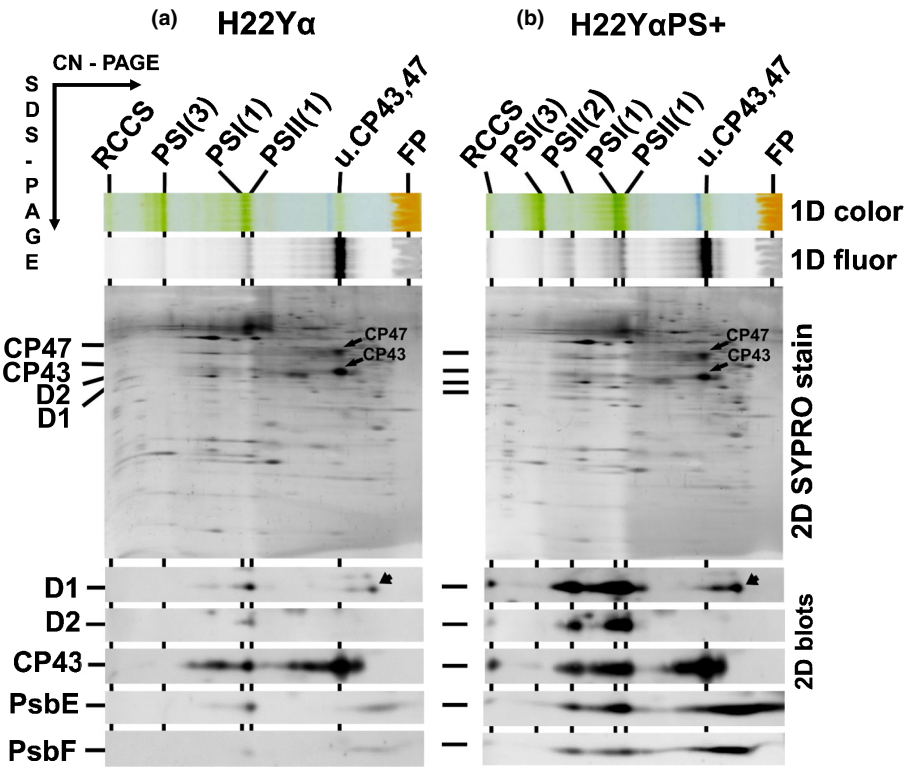

Fig. 9 Two-dimensional PAGE analysis of photosynthetic complexes in (a) the site-directed mutant H22Yα and (b) its corresponding autotrophic transformant H22YαPS+ of *Synechocystis* sp. PCC6803. The experimental conditions were the same as in Fig. 8, designation of complexes as in Fig. 7. Arrows in the blot designate unassembled D1.

led to a 6-fold to 27-fold increase in *psbEFLJ* transcript level compared with the WT (Table 2). In these transformants, *psbD2* (*sll*0927) was upregulated 2- to 6-fold, pointing to a relationship between the expression of Cyt b_{559} and the D2 protein, as *psbD2* encodes this PSII reaction centre protein. Cyt b_{559} is required for the synthesis of D2, and both proteins interact to form a D2-Cyt b_{559} precomplex, an initial PSII assembly intermediate (Müller & Eichacker, 1999; Komenda *et al.*, 2008; Kiss *et al.*, 2019). Our RNA-seq and quantitative RT-PCR analysis also revealed the downregulation of several photosynthesis-related genes, such as *cpcG2* and the *flv4-sll0218-flv2* operon in most or all autotrophic transformant strains. The CpcG2 linker is involved in transferring energy from specific PC rods to PSI (Kondo *et al.*, 2007). Products of the *flv4-sll0218-flv2* operon are involved in dissipating excess energy from PSII (Bersanini *et al.*, 2014; Shimakawa *et al.*, 2015). The function of PSII was impaired in most autotrophic transformant strains, so the decreased transcript levels of *cpcG2* and *flv4-sll0218-flv2* may serve to balance the energy flow between PSII and PSI and optimise the overall photosynthesis efficiency of the autotrophic transformants. The

© 2021 The Authors
New Phytologist © 2021 New Phytologist Foundation

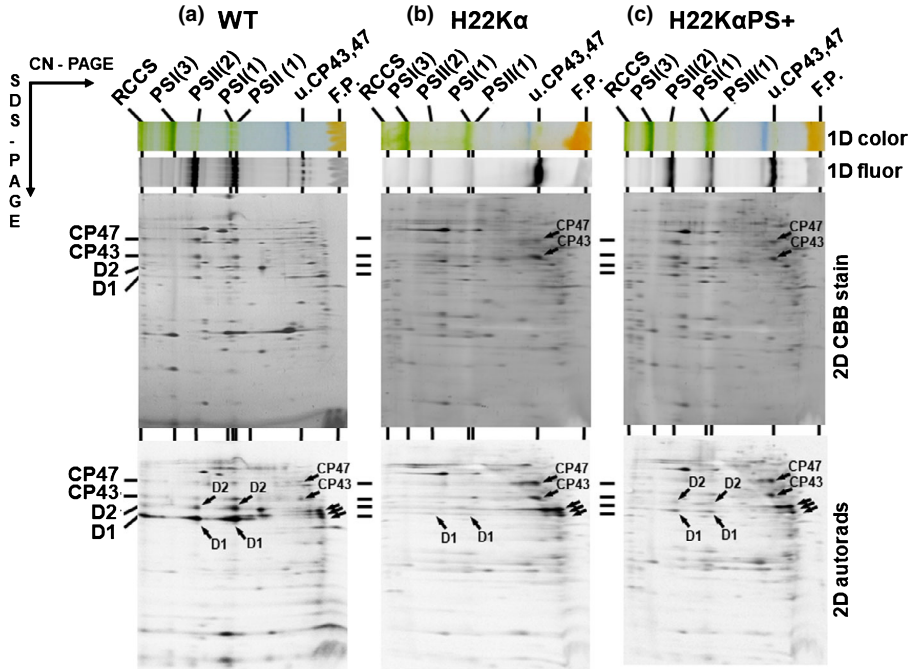

Fig. 10 Two-dimensional PAGE analysis of radioactively labelled photosynthetic complexes in (a) WT, (b) the site-directed mutant H22Kα and (c) its corresponding autotrophic transformant H22KαPS+ of *Synechocystis*. The strains were grown in BG11 containing 5 mM glucose at 40 μmol photons m^{-2} s^{-1} and radioactively labelled with a mixture of [^{35}S] methionine and cysteine. Designations of complexes are as in Fig. 7. Triple arrow indicates labelled unassembled pD1, iD1 and D1 (from top to bottom). Loading was based on the same $OD_{750\ nm}$; in WT, this $OD_{750\ nm}$ corresponded to 4 μg Chl.

above results are consistent with 77 K fluorescence data, which revealed an increase in the PSII to PSI ratio in most autotrophic transformant strains compared with WT cells (Fig. 2b), and native gel electrophoresis data (Fig. 7), which revealed a lower PSI complex levels in the transformants compared with WT.

In addition, many genes involved in high-affinity inorganic carbon transport systems, such as *cmpA/B* (*slr0040/slr0041*), *sbtA/B* (*slr1512/1513*), *cupA* (*sll1734*) and *ndhD3* (*sll1733*), were downregulated in all autotrophic transformants except H22KαPS+, which contained almost WT levels of PSII and oxygen-evolving activity. The expression of the above genes involved in inorganic carbon transport systems in cyanobacteria was regulated by NADPH and α-ketoglutarate concentrations (Daley *et al.*, 2012). Due to impaired photosynthetic activity, these autotrophic transformant strains may be unable to generate sufficient levels of NADPH and ATP synthesis for active inorganic carbon transport.

The results of the analysis of membrane protein complexes in the autotrophic transformants compared with WT and Cyt b_{559} mutants were quite consistent with the negative effect of the axial ligand mutations in each Cyt b_{559} subunit on the accumulation of PsbE and PsbF Cyt b_{559} subunits and the assembly of PSII in the mutant cells. The H22Kα, H22Yβ, and H22Yα strains contained only small amounts of PSII, but transformants with high copy numbers of *psbEFLJ* genes accumulated sufficient amounts of the proteins for the assembly of photochemically active PSII and for autotrophic growth. The transformants still differed in their levels of PSII and in their PSII dimer-to-monomer ratios. H22KαPS+, the strain with the highest oxygen-evolving activity, also contained the highest amount of the PSII dimer, which confirms the crucial function of the dimer in cyanobacterial oxygen evolution. Notably, radioactive labelling of H22KαPS+ revealed that most newly synthesised D1 still remained unassembled. Therefore, compared with the WT, the autotrophic transformants still showed deficient synthesis of D2, the assembly partner of D1.

The results also confirmed that proper coordination of the heme cofactor in Cyt b_{559} is important to the stability of Cyt b_{559} apoproteins and therefore for the assembly of PSII in *Synechocystis* (Pakrasi *et al.*, 1991; Hung *et al.*, 2007, 2010). Surprisingly, in the thermophilic cyanobacterium *Thermosynechococcus elongatus* the constructed H23Aα and H23Mα Cyt b_{559} mutants accumulated the PsbE–PsbF pair in the absence of heme and the accumulation of active PSII was comparable with that in WT cells (Sugiura *et al.*, 2015). The results suggested that, by contrast with *Synechocystis*, in *T. elongatus*, the heme does not affect the stability of Cyt b_{559} apoproteins. Alternatively, it cannot be excluded that the studied *T. elongatus* mutants were in fact 'pseudorevertants' similar to those described in our study, which originated during the process of transformation and autotrophic selection.

Taken together, we revealed a unique mechanism used by cyanobacteria to cope with mutation-induced instability of photosynthetic protein subunits. The mutations in the heme axial ligands of Cyt b_{559} destabilised the PsbE/F apoproteins (possibly due to their altered conformation) and they are quickly degraded. Since the synthesis of D2 is dependent on the presence of the PsbE/F pair, the essential D2 module cannot be formed and PSII assembly is inhibited preventing autotrophic growth of the Cyt b_{559} mutants. The autotrophic transformants compensated for mutation-destabilised Cyt b_{559} subunits via multiple tandem amplifications of chromosomal segments containing the mutated *psbEFLJ* operon. This led to an increase in the transcript level of the mutated Cyt b_{559} gene. The resulting overproduction of the mutation-destabilised Cyt b_{559} subunits allows the D2 synthesis and enables PSII accumulation and photoautotrophic growth of the strains.

© 2021 The Authors
New Phytologist © 2021 New Phytologist Foundation

Acknowledgements

We thank Ghada Ajlani at CNRS, Université Paris-Sud, Université Paris-Saclay, France for the pCB(ΔcpcC1C2) and pCK (ΔcpcBAC1C2) plasmids. We thank Wen-Dar Lin at the Bioinformatics Core Facility of IPMB, Academia Sinica, for assistance with genomic sequencing and RNA-seq analysis and Shu-Jen Chou at the Genomic Core Laboratory of IPMB for genomic DNA and RNA library preparation. We also thank the High Throughput Sequencing Core at Academia Sinica for the PacBio sequencing service. This work was supported by the Czech Science Foundation (project no. 19-29225X), ERC project Photoredesign (no. 854126) (to PS and JK), and the Academia Sinica and the Ministry of Science and Technology in Taiwan (108-2311-B-001-024) (to H-AC).

Author contributions

Y-FC, JK and H-AC designed the study. Y-FC constructed the Type B strains used in this study. Y-FC, H-YF, PS, K-ML and JK performed the research. Y-FC, H-YF, PS, K-ML, JK and H-AC analysed the data. Y-FC, J-MK and H-AC wrote the article. J-MK and H-AC acquired the funding and supervised the project. All authors discussed the results and commented on the article.

ORCID

Yi-Fang Chiu https://orcid.org/0000-0002-6720-2112
Hsiu-An Chu https://orcid.org/0000-0001-8018-4492
Han-Yi Fu https://orcid.org/0000-0001-6864-5866
Josef Komenda https://orcid.org/0000-0003-4588-0382
Keng-Min Lin https://orcid.org/0000-0002-1382-512X
Petra Skotnicová https://orcid.org/0000-0002-6077-0256

Data availability

The whole-genome sequencing datasets of autotrophic transformants were deposited in the NCBI SRA database with accession number PRJNA753222.

References

Andersson DI, Hughes D. 2013. Gene amplification and adaptive evolution in bacteria. *Annual Review of Genetics* **43**: 167–195.

Andrizhiyevskaya EG, Chojnicka A, Bautista JA, Diner BA, van Grondelle R, Dekker JP. 2005. Origin of the F685 and F695 fluorescence in photosystem II. *Photosynthesis Research* **84**: 173–180.

Barber J. 2006. Photosystem II: an enzyme of global significance. *Biochemical Society Transactions* **34**: 619–631.

Barber J, De Las RJ. 1993. A functional model for the role of cytochrome b_{559} in the protection against donor and acceptor side photoinhibition. *Proceedings of the National Academy of Sciences, USA* **90**: 10942–10946.

Bersanini L, Battchikova N, Jokel M, Rehman A, Vass I, Allahverdiyeva Y, Aro E-M. 2014. Flavodiiron protein Flv2/Flv4-related photoprotective mechanism dissipates excitation pressure of PSII in cooperation with phycobilisomes in cyanobacteria. *Plant Physiology* **164**: 805–818.

Boehm M, Romero E, Reisinger V, Yu J, Komenda J, Eichacker LA, Dekker JP, Nixon PJ. 2011. Investigating the early stages of photosystem II assembly in *Synechocystis* sp. *PCC 6803* isolation of CP47 and CP43 complexes. *Journal of Biological Chemistry* **286**: 14812–14819.

Bondarava N, De Pascalis L, Al-Babili S, Goussias C, Golecki JR, Beyer P, Bock R, Krieger-Liszkay A. 2003. Evidence that cytochrome b_{559} mediates the oxidation of reduced plastoquinone in the dark. *Journal of Biological Chemistry* **278**: 13554–13560.

Büsch A, Friedrich B, Cramm R. 2002. Characterization of the *norB* gene encoding nitric oxide reductase in the nondenitrifying cyanobacterium *Synechocystis* sp. strain PCC6803. *Applied Environmental Microbiology* **68**: 668–672.

Calzadilla PI, Kirilovsky D. 2020. Revisiting cyanobacterial state transitions. *Photochemical & Photobiological Science* **19**: 585–603.

Chin C-S, Alexander DH, Marks P, Klammer AA, Drake J, Heiner C, Clum A, Copeland A, Huddleston J, Eichler EE *et al.* 2013. Nonhybrid, finished microbial genome assemblies from long-read SMRT sequencing data. *Nature Methods* **10**: 563–569.

Chu H-A, Chang I, Shen C, Chen Y-H, Wang H, Huang L, Yeh K. 2012. Photosynthetic properties and photosystem stoichiometry of *in vitro*-grown juvenile, adult, and rejuvenated *Sequoia sempervirens* (D. Don) Endl. *Botanical Studies* **53**: 223–227.

Chiu Y-F, Chen Y-H, Roncel M, Dilbeck PL, Huang J-Y, Ke S-C, Ortega JM, Burnap RL, Chu H-A. 2013. Spectroscopic and functional characterization of cyanobacterium *Synechocystis* PCC 6803 mutants on the cytoplasmic-side of cytochrome b_{559} in photosystem II. *Biochimica et Biophysica Acta* **1827**: 507–519.

Chu H-A, Chiu Y-F. 2016. The roles of cytochrome b_{559} in assembly and photoprotection of photosystem II revealed by site-directed mutagenesis studies. *Frontiers in Plant Science* **6**: 1261–1267.

Chu H-A, Nguyen AP, Debus RJ. 1994. Site-directed photosystem II mutants with perturbed oxygen-evolving properties. 1. Instability or inefficient assembly of the manganese cluster in vivo. *Biochemistry* **33**: 6137–6149.

Daley SME, Kappell AD, Carrick MJ, Burnap RL. 2012. Regulation of the cyanobacterial CO_2-concentrating mechanism involves internal sensing of $NADP^+$ and α-ketogutarate levels by transcription factor CcmR. *PLoS ONE* **7**: e41286–e41295.

Dobáková M, Tichý M, Komenda J. 2007. Role of the psbI protein in photosystem II assembly and repair in the cyanobacterium *Synechocystis* sp. PCC 6803. *Plant Physiology* **145**: 1681–1691.

Elliott KT, Cuff LE, Neidle EL. 2013. Copy number change: evolving views on gene amplification. *Future Microbiology* **8**: 887–899.

He Q, Dolganov N, Björkman O, Grossman AR. 2001. The high light-inducible polypeptides in *Synechocystis* PCC6803: expression and function in high light. *Journal of Biological Chemistry* **276**: 306–314.

Huang J-Y, Chiu Y-F, Ortega JM, Wang H-T, Tseng T-S, Ke S-C, Roncel M, Chu H-A. 2016. Mutations of cytochrome b_{559} and *psbJ* on and near the Q_C site in photosystem II influence the regulation of short-term light response and photosynthetic growth of the cyanobacterium *Synechocystis* sp. PCC 6803. *Biochemistry* **55**: 2214–2226.

Huang J-Y, Hung N-T, Lin K-M, Chiu Y-F, Chu H-A. 2018. Regulating photoprotection improves photosynthetic growth and biomass production in Q_C-site mutant cells of the cyanobacterium *Synechocystis* sp. PCC 6803. *Photosynthetica* **56**: 192–199.

Hung C-H, Huang J-Y, Chiu Y-F, Chu H-A. 2007. Site-directed mutagenesis on the heme axial-ligands of cytochrome b_{559} in photosystem II by using cyanobacteria *Synechocystis* PCC 6803. *Biochimica et Biophysica Acta* **1767**: 686–693.

Hung C-H, Hwang H-J, Chen Y-H, Chiu Y-F, Ke S-C, Burnap RL, Chu H-A. 2010. Spectroscopic and functional characterizations of cyanobacterium *Synechocystis* PCC 6803 mutants on and near the heme axial ligand of cytochrome b_{559} in photosystem II. *Journal of Biological Chemistry* **285**: 5653–5663.

Kiss É, Knoppová J, Aznar GP, Pilný J, Yu J, Halada P, Nixon PJ, Sobotka R, Komenda J. 2019. A photosynthesis-specific rubredoxin-like protein is required for efficient association of the D1 and D2 proteins during the initial steps of photosystem II assembly. *Plant Cell* **31**: 2241–2258.

Komenda J, Barker M, Kuviková S, de Vries R, Mullineaux CW, Tichý M, Nixon PJ. 2006. The ftsH protease *slr0228* is important for quality control of photosystem II in the thylakoid membrane of *Synechocystis* sp. PCC 6803. *Journal of Biological Chemistry* **281**: 1145–1151.

© 2021 The Authors
New Phytologist © 2021 New Phytologist Foundation

Komenda J, Nickelsen J, Tichý M, Prášil O, Eichacker LA, Nixon PJ. 2008. The cyanobacterial homologue of HCF136/YCF48 is a component of an early photosystem II assembly complex and is important for both the efficient assembly and repair of photosystem II in *Synechocystis* sp. PCC 6803. *Journal of Biological Chemistry* **283**: 22390–22399.

Komenda J, Reisinger V, Muller BC, Dobakova M, Granvogl B, Eichacker LA. 2004. Accumulation of the D2 protein is a key regulatory step for assembly of the photosystem II reaction center complex in *Synechocystis* PCC 6803. *Journal of Biological Chemistry* **279**: 48620–48629.

Kondo K, Ochiai Y, Katayama M, Ikeuchi M. 2007. The membrane-associated CpcG2-phycobilisome in *Synechocystis*: a new photosystem I antenna. *Plant Physiology* **144**: 1200–1210.

Lamb JJ, Rokke G, Hohmann-Marriott MF. 2018. Chlorophyll fluorescence emission spectroscopy of oxygenic organisms at 77 K. *Photosynthetica* **56**: 105–124.

Morais F, Barber J, Nixon PJ. 1998. The chloroplast-encoded α subunit of cytochrome b_{559} is required for assembly of the photosystem two complex in both the light and the dark in *Chlamydomonas reinhardtii*. *Journal of Biological Chemistry* **273**: 29315–29320.

Müller B, Eichacker LA. 1999. Assembly of the D1 precursor in monomeric photosystem II reaction center precomplexes precedes chlorophyll*a* triggered accumulation of reaction center II in barley etioplasts. *Plant Cell* **11**: 2365–2377.

Nickelsen J, Rengstl B. 2013. Photosystem II assembly: from cyanobacteria to plants. *Annual Review of Plant Biology* **64**: 609–635.

Nixon PJ, Michoux F, Yu J, Boehm M, Komenda J. 2010. Recent advances in understanding the assembly and repair of photosystem II. *Annals of Botany* **106**: 1–16.

Ohad I, Dal Bosco C, Herrmann RG, Meurer J. 2004. Photosystem II proteins PsbL and PsbJ regulate electron flow to the plastoquinone pool. *Biochemistry* **43**: 2297–2308.

Omata T, Price GD, Badger MR, Okamura M, Gohta S, Ogawa T. 1999. Identification of an ATP-binding cassette transporter involved in bicarbonate uptake in the cyanobacterium *Synechococcus* sp. strain PCC 7942. *Proceedings of the National Academy of Sciences, USA* **96**: 13571–13576.

Pakrasi HB, Ciechi PD, Whitmarsh J. 1991. Site directed mutagenesis of the heme axial ligands of cytochrome b_{559} affects the stability of the photosystem II complex. *EMBO Journal* **10**: 1619–1627.

Pakrasi HB, Williams JG, Arntzen CJ. 1988. Targeted mutagenesis of the *psbE* and *psbF* genes blocks photosynthetic electron transport: evidence for a functional role of cytochrome b_{559} in photosystem II. *EMBO Journal* **7**: 325–332.

Reams A, Roth J. 2015. Mechanisms of gene duplication and amplification. *Cold Spring Harbor Perspectives in Biology* **7**: a016592–a016616.

Shimakawa G, Shaku K, Nishi A, Hayashi R, Yamamoto H, Sakamoto K, Makino A, Miyake C. 2015. Flavodiiron2 and flavodiiron 4 proteins mediate an oxygen-dependent alternative electron flow in *Synechocystis* sp. PCC 6803 under CO_2-limited conditions. *Plant Physiology* **167**: 472–480.

Shinopoulos KE, Brudvig GW. 2012. Cytochrome b_{559} and cyclic electron transfer within photosystem II. *Biochimica et Biophysica Acta* **1817**: 66–75.

Sugiura M, Nakamura M, Koyama K, Boussac A. 2015. Assembly of oxygen-evolving photosystem II efficiently occurs with the apo-Cytb_{559} but the holo-Cytb_{559} accelerates the recovery of a functional enzyme upon photoinhibition. *Biochimica et Biophysica Acta* **1847**: 276–285.

Swiatek M, Regel RE, Meurer J, Wanner G, Pakrasi HB, Ohad I, Herrmann RG. 2003. Effects of selective inactivation of individual genes for low-molecular-mass subunits on the assembly of photosystem II, as revealed by chloroplast transformation: the *psbEFLJ* operon in *Nicotiana tabacum*. *Molecular Genetics and Genomics* **268**: 699–710.

Thomas JC, Ughy B, Lagoutte B, Ajlani G. 2006. A second isoform of the ferredoxin:NADP oxidoreductase generated by an in-frame initiation of translation. *Proceedings of the National Academy of Sciences, USA* **103**, 18368–18373.

Tichy M, Beckova M, Kopecna J, Noda J, Sobotka R, Komenda J. 2016. Strain of *Synechocystis* PCC 6803 with aberrant assembly of photosystem II contains tandem duplication of a large chromosomal region. *Frontiers in Plant Science* **7**: 648–657.

Tokumaru Y, Uebayashi K, Toyoshima M, Osanai T, Matsuda F, Shimizu H. 2018. Comparative targeted proteomics of the central metabolism and photosystems in SigE mutant strains of *Synechocystis* sp. PCC 6803. *Molecules* **23**: 1051.

Ughy B, Ajlani G. 2004. Phycobilisome rod mutants in *Synechocystis* sp. strain PCC6803. *Microbiology* **150**: 4147–4156.

Umena Y, Kawakami K, Shen JR, Kamiya N. 2011. Crystal structure of oxygen-evolving photosystem II at a resolution of 1.9 Å. *Nature* **473**: 55–60.

Wang C, Sun B, Zhang X, Huang X, Zhang M, Guo H, Chen X, Huang F, Chen T, Mi H *et al.* 2019. Structural mechanism of the active bicarbonate transporter from cyanobacteria. *Nature Plants* **5**: 1184–1193.

Zabret J, Bohn S, Schuller SK, Arnolds O, Möller M, Meier-Credo J, Liauw P, Chan A, Tajkhorshid E, Langer JD *et al.* 2021. Structural insights into photosystem II assembly. *Nature Plants* **7**: 524–538.

Zhang P, Battchikova N, Jansen T, Appel J, Ogawa T, Aro EM. 2004. Expression and functional roles of the two distinct NDH-1 complexes and the carbon acquisition complex NdhD3/NdhF3/CupA/Sll1735 in *Synechocystis* sp PCC 6803. *Plant Cell* **16**: 3326–3340.

Supporting Information

Additional Supporting Information may be found online in the Supporting Information section at the end of the article.

Fig. S1 Photoautotrophic growth curves of wild-type and autotrophic transformant cells.

Fig. S2 Mapping of Illumina sequencing reads of autotrophic transformants to the reference sequences of the pAC559Em plasmid.

Fig. S3 Two-dimensional PAGE analysis of photosynthetic complexes in the site-directed mutant H22Yβ and its corresponding autotrophic transformant H22YβPS+ of *Synechocystis*.

Table S1 Primers used for droplet digital PCR analysis.

Table S2 Sequences of the gene-specific primers used in real-time-PCR assays.

Table S3 Verification of copy number variation of *cpcC1C2* in the wild-type and autotrophic transformants by droplet digital PCR.

Table S4 The reads/coverage of mutation sites of H22α or H22β in autotrophic transformants obtained by whole-genome sequencing.

Table S5 Common differentially expressed genes in autotrophic transformant cells.

Please note: Wiley Blackwell are not responsible for the content or functionality of any Supporting Information supplied by the authors. Any queries (other than missing material) should be directed to the *New Phytologist* Central Office.

© 2021 The Authors
New Phytologist © 2021 New Phytologist Foundation